


Cite this: *RSC Adv.*, 2022, 12, 7284

# Cobalt-loaded cherry core biochar composite as an effective heterogeneous persulfate catalyst for bisphenol A degradation†

Li Li,<sup>a</sup> Yuanyuan Zhang,<sup>b</sup> Shuangshuang Yang,<sup>a</sup> Shengxiao Zhang,<sup>a</sup>  <sup>✉</sup> Qiang Xu,<sup>a</sup> Pinzhu Chen,<sup>a</sup> Yaxuan Du<sup>a</sup> and Yuxin Xing<sup>a</sup>

Persulfate (PS)-based advanced oxidation processes have drawn tremendous attention for the degradation of recalcitrant pollutants, and cobalt composites are effective for PS activation to generate reactive species. In this study, composites of cobalt species loaded on cherry core-derived biochar (Co/C) were prepared with a one-step pyrolysis method. The Co/C catalyst was applied as a catalyst for PS activation to degrade bisphenol A (BPA). Factors influencing the degradation efficiency were examined, including the ratio of raw materials, Co/C and PS dosages, temperature, and solution pH. The Co/C catalyst prepared when the ratio of raw material was 1 : 1 (Co/C-50) could efficiently activate both peroxymonosulfate (PMS) and peroxydisulfate (PDS). When the initial concentration of BPA was 20 mg L<sup>-1</sup>, complete removal of BPA was achieved in the Co/C-50-PMS and Co/C-50-PDS systems within 8 min and 10 min, respectively. More than 70% of BPA could be mineralized in the Co/C-50-PS system. The free radical quenching experiments demonstrated that in the Co/C-50-PS system, the degradation of BPA was achieved through free radical, surface-bound free radical, and non-free radical pathways. The successful preparation of the Co/C-50-PS catalyst broadens the application of cobalt-based carbon materials in the activation of PS to remove organic pollutants.

Received 21st December 2021  
Accepted 17th February 2022

DOI: 10.1039/d1ra09236g

rsc.li/rsc-advances

## 1. Introduction

Bisphenol A (BPA) is one of the most common endocrine disrupting compounds that bind to estrogen receptors in the body and interfere with the synthesis, metabolism and activity of normal oestrin,<sup>1</sup> and it is extensively used in industrial processes as a plasticizer, such as in plastic manufacturing, adhesives, elasticizers, and hardeners.<sup>2</sup> Due to its wide application, it is frequently detected in drinking water, surface water, wastewater and even treatment wastewater. These pollutants are toxic, carcinogenic, teratogenic and mutagenic.<sup>3–7</sup> For example, BPA can increase the risk of developing ovarian cancer, prostate cancer, asthma and leukemia.<sup>8</sup> The physical and chemical properties of BPA are stable, and it is difficult to remove BPA effectively by biodegradation. Therefore, there is an urgent need to develop effective degradation technology for BPA removal.

A variety of remediation technologies have been developed for BPA degradation, among which advanced oxidation processes (AOPs) have been paid increasing attention due to their easy operation, strong oxidation degradation ability, and lower secondary pollution.<sup>9</sup> Advanced oxidation technology based on the sulfate radical (SO<sub>4</sub><sup>•-</sup>) is a new type of technology developed in recent years to treat refractory organic pollutants.<sup>10</sup> SO<sub>4</sub><sup>•-</sup> is mainly produced by the activation of persulfates, which include peroxymonosulfate (PMS) and peroxydisulfate (PDS), both of which have unstable O–O bonds and are prone to external electron fracture.<sup>11</sup> The standard redox potential of SO<sub>4</sub><sup>•-</sup> ( $E^0 = 2.5\text{--}3.1\text{ V}$ ) is higher than that of <sup>•</sup>OH ( $E^0 = 1.8\text{--}2.7\text{ V}$ ); therefore, SO<sub>4</sub><sup>•-</sup> is a strong oxidant, and the half-life of SO<sub>4</sub><sup>•-</sup> (about 30–40 μs) is much higher than that of <sup>•</sup>OH (less than 1 μs), which indicates that SO<sub>4</sub><sup>•-</sup> is more stable and has a longer contact time with potential pollutants compared to <sup>•</sup>OH.<sup>12</sup> Moreover, SO<sub>4</sub><sup>•-</sup> can maintain high activity in a wide range of solution pH values, especially in neutral or alkaline conditions, showing higher activity than <sup>•</sup>OH.<sup>13</sup> Therefore, compared with other traditional water treatment technologies, AOPs based on SO<sub>4</sub><sup>•-</sup> (S-AOPs) have the advantages of high efficiency, rapidity, thoroughness, low selectivity, and mild reaction conditions,<sup>14</sup> and have wide application prospects in the field of environmental pollution remediation and treatment.

SO<sub>4</sub><sup>•-</sup> was produced mainly by activating persulfate, and common activation methods include heat,<sup>15</sup> microwave,<sup>16,17</sup>

<sup>a</sup>School of Chemistry and Materials Science, Collaborative Innovation Center of Shandong Province for High Performance Fibers and Their Composites, Ludong University, Yantai 264025, Shandong province, China. E-mail: beijingzxsx@163.com; Fax: +086 0535-6695905; Tel: +086 0535-6696162

<sup>b</sup>Environmental Monitor Station of Yantai, No. 118, Qingnian South Road, Yantai 264000, Shandong province, China

† Electronic supplementary information (ESI) available. See DOI: 10.1039/d1ra09236g



ultrasound,<sup>18</sup> UV radiation,<sup>19,20</sup> transition metal,<sup>21,22</sup> carbon composites,<sup>23,24</sup> and alkali.<sup>25</sup> Transition metal activation has the advantages of low energy consumption, high efficiency, and mild reaction conditions. Some metal catalysts (such as cobalt, copper, iron, and manganese) been demonstrated to be effective in activating persulfate.<sup>26–28</sup> Among them, cobalt is considered to be the most effective non-noble metal catalyst for persulfate activation. However, homogeneous cobalt ions added to a solution are not easy to recover, leading to secondary contamination. Therefore, heterogeneous Co-based catalysts gradually substituted with homogeneous Co ions have been widely applied to activate PS. To date, scholars have studied a variety of heterogeneous cobalt-based catalysts, mainly including cobalt oxide (CoO, CoO<sub>2</sub>, Co<sub>2</sub>O<sub>3</sub>, CoO(OH), Co<sub>3</sub>O<sub>4</sub>), spinel cobalt ferrite (CoFe<sub>2</sub>O<sub>4</sub>) and supported cobalt catalysts (supported substrates include MO<sub>x</sub> metal oxides, molecular sieves, carbon materials, and MOFs).<sup>29</sup> Biochar is a new kind of low-cost carbonaceous material that is produced by low-cost waste biomass residues. Due to its high specific surface area, excellent electronic conduction properties and good stability, biochar is a promising candidate for loading of metal nanoparticles. Tian *et al.*<sup>30</sup> impregnated corn straw by hydrothermal carbonization in CoCl<sub>2</sub> solution, and they successfully loaded Co<sub>3</sub>O<sub>4</sub> nanoparticles on the surface of biochar to manufacture a Co-BC composite for activating PMS to degrade sulfamethazine in aqueous solution.

In this study, Co/C composites were manufactured by using cherry core powder and CoCl<sub>2</sub>·6H<sub>2</sub>O to activate PS to degrade pollutants, which provides an available method for large-scale production and application of environmental materials in the AOPs field. Cherry core biochar composites supported with Co species were synthesized and used as catalysts for activated persulfate to degrade BPA. The influencing factors of the degradation of BPA by the Co–C composites activating PS were investigated, and the reuse and practical application of the materials were examined.

## 2. Materials and methods

### 2.1 Chemicals and reagents

The chemicals and reagents are shown in Text S1.†

### 2.2 Synthesis of Co/C

CoCl<sub>2</sub>·6H<sub>2</sub>O and cherry kernel powder were scattered in 50 mL ethanol and heated to 120 °C with magnetic stirring until dried. After steam-drying, the solid matter was removed and ground in a mortar. It was calcined in a tubular furnace under argon atmosphere for 5 h at 800 °C. The amounts of CoCl<sub>2</sub>·6H<sub>2</sub>O and cherry stone were changed to make Co/C materials with different cobalt contents; they were labeled as C, Co/C-10, Co/C-20, Co/C-30, Co/C-40, Co/C-50, Co/C-60, Co/C-70, Co/C-80 and Co/C-90, respectively. The specific preparation method is presented in Table S1.†

### 2.3 Material characterization

The characterization methods of the materials are shown in Text S2.†

## 2.4 Degradation experiments

The catalytic degradation of BPA was carried out in a glass conical flask. Certain amounts of Co/C-50 and persulfate were added to 100 mL BPA solution (20 mg L<sup>−1</sup>) and oscillated for 30 min in a water bath thermostatic oscillator at 30 °C. The initial pH was regulated with HCl and NaOH solution. Within a certain time interval, 3 mL solution was taken out and mixed with 3 mL methanol to quench the reaction. The mixture was centrifuged, and the supernatant was taken for analysis. The concentration of BPA was analyzed by high performance liquid chromatography (HPLC, UltiMate 3000, US). The mobile phase consisted of methanol and 0.5% phosphoric acid (volume ratio: 80 : 20), the flow rate was 1 mL min<sup>−1</sup>, and the column temperature was 30 °C. In the recyclability test, Co/C-50 was separated and recovered with a magnet (Text S3 and Fig. S1†), and then simple SnCl<sub>2</sub> washing and water washing regeneration were carried out for the next experiment. A TOC-L analyzer (Shimadzu, Japan) was used to determine the total organic carbon (TOC) of the aqueous solutions.

## 3. Results and discussion

### 3.1 Characterization of Co/C

**3.1.1 XRD and Raman spectral characterization.** Five catalysts (activated carbon, Co/C-20, Co/C-50, Co/C-60 and Co/C-90) were characterized by XRD and Raman spectra. The diffraction peaks of Co<sup>0</sup> (111), (101), (200) and (220) were at 44.22°, 47.57°, 51.52° and 75.85°, respectively (JCPDS no.15-0806 and no.05-0727). This indicated that Co<sup>0</sup> nanocrystals appeared in the catalyst (Fig. 1a), and their formation was due to the reduction of Co<sup>2+</sup> by the biomass activated carbon during calcination. With the increase of Co content, the diffraction peak of the carbon (002) crystal plane became smaller and narrower; this indicated that the addition of Co increased the graphitization degree of activated carbon, and the graphitization degree increased with the increase of the Co content. The enhanced graphitization degree was favorable for electron transfer.<sup>31</sup> These results indicated that the Co/C catalysts were more conducive to PS activation than activated carbon. Meanwhile, the four crystal faces of CoO (111), (200), (220) and (311) at 36.50°, 42.40°, 61.52° and 73.70°, respectively (JCPDS no. 43-1004), were also detected in the XRD patterns. In the Raman spectrograms (Fig. 1b), D and G peaks appeared in all five materials, and the I<sub>D</sub>/I<sub>G</sub> value was also used to measure the graphitization degree of the five catalysts. As can be seen from Fig. 1b, the I<sub>D</sub>/I<sub>G</sub> value decreases with the increase of Co content. This indicates that the graphitization degree of the material increases with the increase of Co content, which is in agreement with the XRD results.

**3.1.2 FT-IR characterization.** The four Co/C materials were characterized by Fourier transform infrared spectroscopy (FT-IR). As shown in Fig. S2,† the strong and wide absorption peak at 3432 cm<sup>−1</sup> was the stretching vibration peak of O–H; the absorption peaks near 2922 cm<sup>−1</sup> and 2853 cm<sup>−1</sup> were the stretching vibration peaks of C–H; at 1631 cm<sup>−1</sup>; the slightly stronger absorption peaks were C=C and C=O stretching

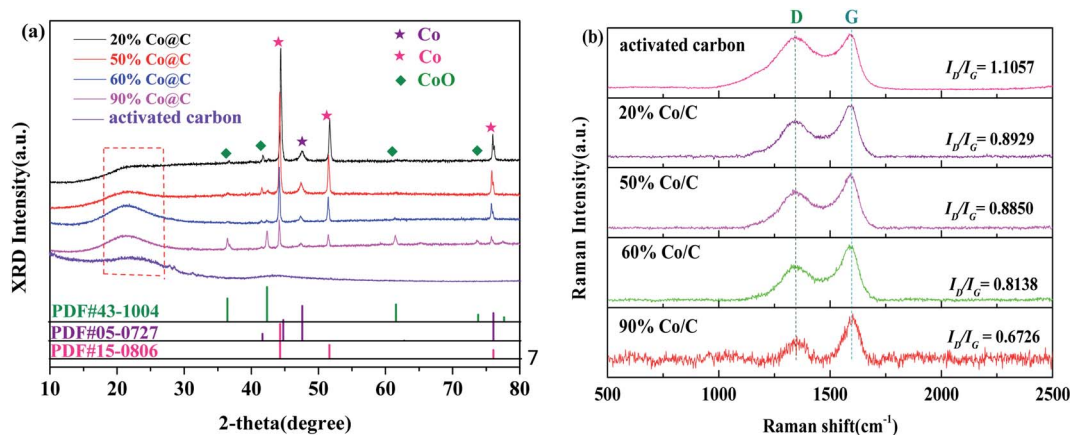


Fig. 1 XRD patterns (a) and Raman spectra (b) of the five different samples.

vibration peaks; the peak at 1384 cm<sup>-1</sup> corresponded to the characteristic peak of O=C=O; and the stretching vibration peaks of C-C and C-O appeared at 1114 cm<sup>-1</sup>. These findings demonstrated that the Co/C catalysts had abundant oxygen-containing and carbon-containing functional groups. The Co-O peaks near 660 cm<sup>-1</sup> and 570 cm<sup>-1</sup> indicated that the Co/C catalysts contained CoO,<sup>32</sup> which was consistent with the XRD results.

**3.1.3 XPS characterization.** The valence of Co/C was characterized by XPS. In the XPS diagrams of Co/C-20, Co/C-50, Co/C-60 and Co/C-90 (Fig. 2a), the photoelectron characteristic peaks of O 1s and C 1s in activated carbon were observed, and

a peak of Co 2p was detected at 780.34 eV, indicating that Co element was successfully loaded onto the carbon substrate. The C 1s fine spectrum of Co/C-50 (Fig. 2b and c) showed that the main forms of C included C=C/C-C (284.5 eV), C-O (286.1 eV), C=O (286.56 eV), and O-C=O (289.2 eV),<sup>33,34</sup> and O 1s exhibited not only O-C (531.3 eV), O=C (532.5 eV), and O-C=O (533.5 eV), but also the peak of the Co-O bond at 530.1 eV as the main oxygen-containing functional groups.<sup>35</sup> Moreover, we decomposed the peak of Co 2p in detail. As shown in Fig. 2d, the Co 2p spectrum consisted of two spin orbit peaks and two satellite peaks of Co 2p<sub>1/2</sub> and Co 2p<sub>3/2</sub>, and the peaks of Co<sup>0</sup> (778.8 eV, 794.1 eV) and Co<sup>2+</sup> (780.5 eV, 796.5 eV) were found in Co 2p<sub>1/2</sub>

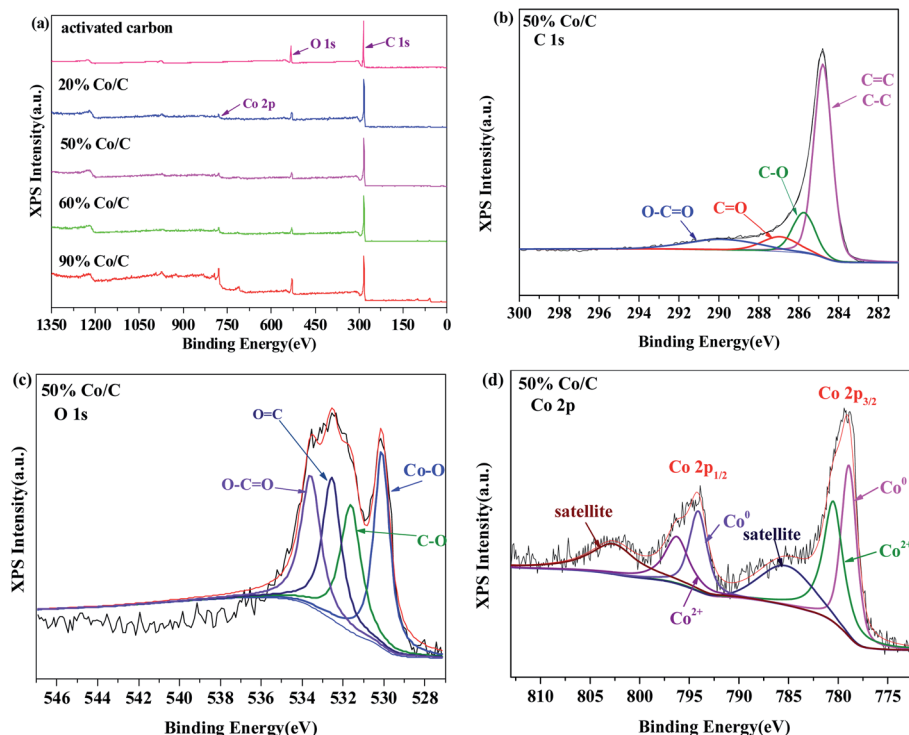


Fig. 2 XPS spectra of the as-prepared catalysts: (a) survey, (b) C 1s, (c) O 1s, (d) Co 2p.





and Co 2p<sub>3/2</sub>,<sup>36</sup> confirming the existence of Co and CoO crystals; this was consistent with the XRD results.

**3.1.4 HR-TEM characterization.** The morphologies and lattice structures of the Co/C-50 catalysts were analyzed by HR-TEM. The TEM images (Fig. 3a) exhibited that the biomass activated carbon was distributed in sheets, and it had a very thin layered structure; moreover, some areas showed multi-layer stacking. Spherical CoO<sub>x</sub> nanoparticles (10–50 nm) were dispersed on the carbon substrate, and no isolated CoO<sub>x</sub> nanoparticles appeared outside the carbon substrate, which was beneficial to the dispersion and stability of the CoO<sub>x</sub> nanoparticles. HR-TEM images (Fig. 3b) were used to clarify the crystal types and crystal faces of CoO<sub>x</sub>. The crystal plane spacings of Co<sup>0</sup> (101) and CoO (111) were 0.191 nm and 0.245 nm, respectively. Selected area electron diffraction (SAED) showed the single crystal characteristic of the Co<sup>0</sup> and CoO nanoparticles. The results indicated that both Co<sup>0</sup> and CoO existed in Co/C-50, which was consistent with the results of XPS and XRD. The Co<sup>0</sup> and CoO lattice structures were arranged in an orderly manner and formed a good combination with the carbon substrate. Element mapping images (Fig. 3c) showed that Co/C-50 was composed of C, O and Co, and Co and O were distributed on the carbon substrate. ICP-MS (NexION 300X) was used to determine the contents of cobalt in the catalysts (Table S2†), and the results exhibited the same trend as the ratios of raw materials.

## 3.2 Catalytic degradation experiment

**3.2.1 Effects of different mass ratios of Co/C.** The performance of Co/C with different mass ratios to activate PS and degrade BPA was investigated. The pseudo-first-order kinetics model was used to fit the degradation data, and the equation was as follows (eqn (1)):

$$\ln(c_t/c_0) = -k_1 t \quad (1)$$

where  $k_1$  (min<sup>−1</sup>) is the kinetics rate constant,  $t$  (min) is the reaction time, and  $c_t$  and  $c_0$  (mg L<sup>−1</sup>) are the concentrations of BPA at times  $t$  and 0, respectively.

Compared with the other Co supported catalysts, activated carbon-activated PS had the lowest degradation efficiency of BPA (Fig. 4). The load of Co on the activated carbon could remarkably improve the catalytic activity. In addition, as the content of Co increased from 0% to 50%, the degradation efficiency of BPA was enhanced. However, when the Co content was over 50%, the degradation efficiency of BPA was attenuated with the increase of the Co content. The  $k_1$  values showed a similar trend. When the Co content reached 50%, the maximum value of  $k_1$  occurred (PMS: 0.517 min<sup>−1</sup>, PDS: 0.586 min<sup>−1</sup>). This was mainly due to the limited active sites of the catalyst when the Co content was too low. With the increase of Co content, more active sites could be provided for persulfate activation. However, when the Co content outstripped 50%, excessive metal ions gathered in the catalytic center, resulting in decreases of the catalytic activity<sup>37</sup> and degradation efficiency. This indicated that the appropriate proportion of Co loading could promote the catalytic activity of Co/C.<sup>33</sup> Because Co/C-50 showed the best catalytic activity and had a high specific surface area (262.5032 m<sup>2</sup> g<sup>−1</sup>) (Text S4 and Fig. S3†), the Co/C-50 catalyst was selected for investigation in the following experimental studies. Table S3† shows a comparison of the BPA degradation efficiency of different catalysts. The results indicated that the Co/C-50 catalyst prepared in this study has a competitive advantage in BPA degradation.

**3.2.2 Effects of different catalyst dosages.** Fig. 5 shows the effects of the catalyst dosage on BPA degradation. When the amount of Co/C-50 was 0, the BPA removal efficiencies of PMS and PDS were only 0.95% and 2.02%, respectively. These findings suggested that PMS and PDS alone had little influence on

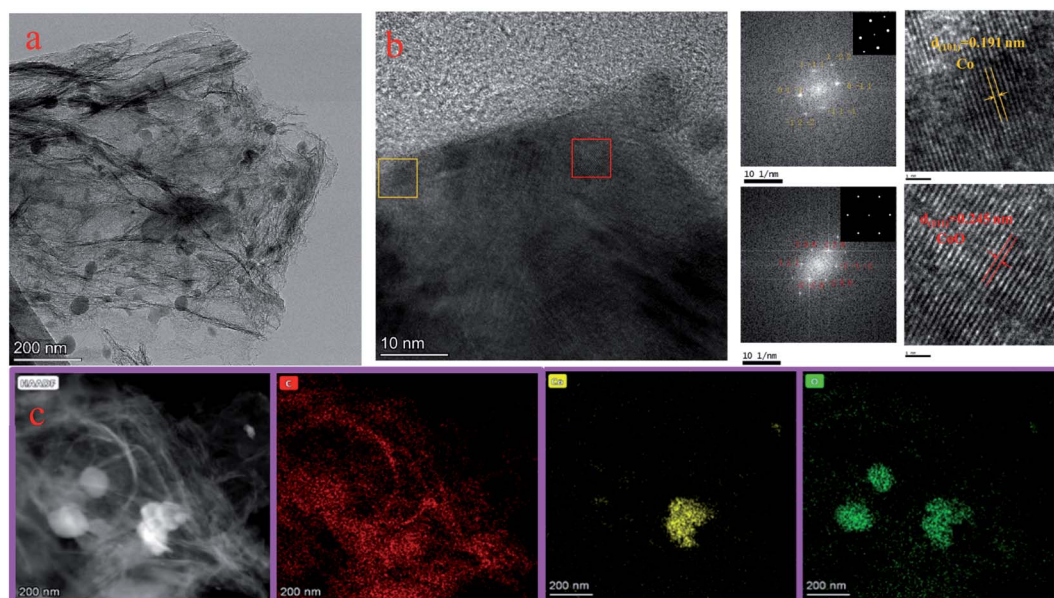


Fig. 3 (a) TEM image, (b) HR-TEM image, and (c) EDS mapping of Co/C-50.

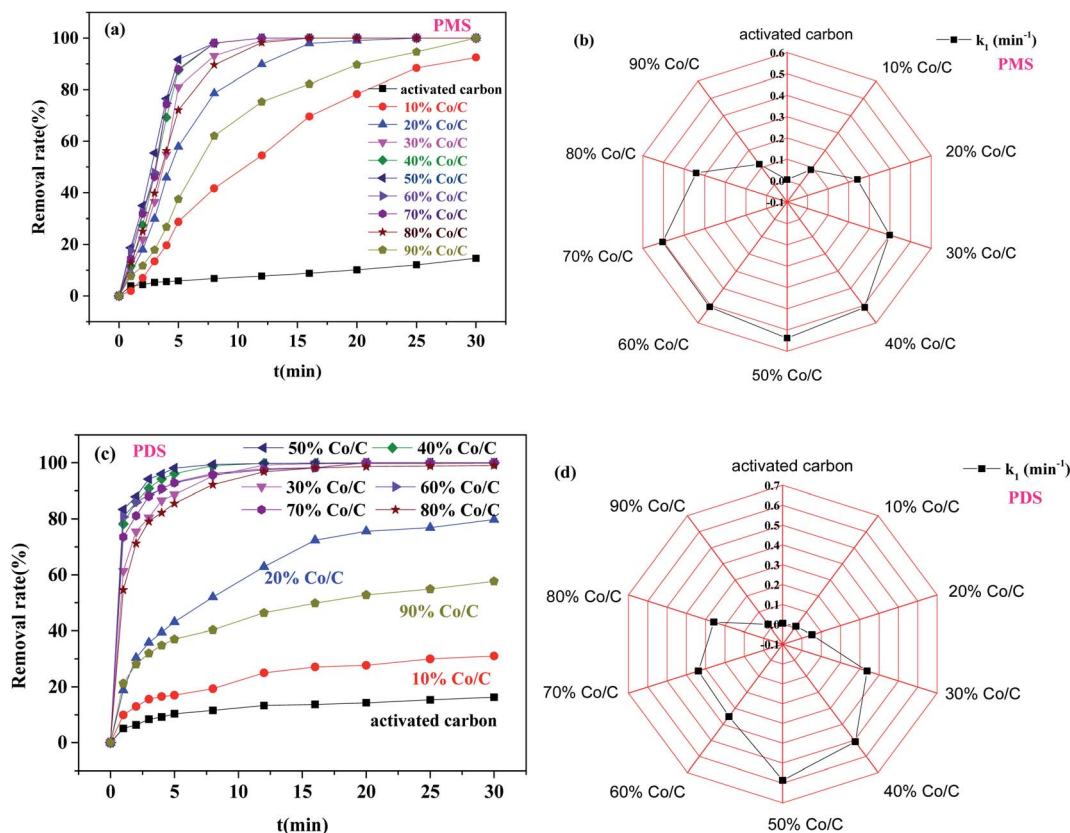
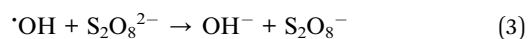
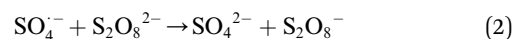


Fig. 4 The effects of different mass ratios of Co/C on BPA degradation: removal efficiency of BPA with (a) PMS and (c) PDS; the pseudo-first-order kinetic constants of (b) PMS and (d) PDS (PMS system:  $m_{\text{catalyst}} = 0.0050$  g,  $[\text{PMS}] = 0.25$  g L $^{-1}$ ; PDS system:  $m_{\text{catalyst}} = 0.04$  g,  $[\text{PDS}] = 1.0$  g L $^{-1}$ ,  $[\text{BPA}] = 20$  mg L $^{-1}$ ,  $T = 30$  °C).

the BPA degradation due to their own oxidation.<sup>38</sup> In the Co/C-50-PMS system (Fig. 5a and b), the BPA degradation efficiency increased rapidly when the Co/C-50 dosage increased from 0 to 0.0050 g, and the  $k_1$  value increased from  $6.90 \times 10^{-4}$  to  $0.537$  min $^{-1}$ . This phenomenon can be attributed to the growth of catalytic active sites, which accelerated the degradation efficiency. However, when the dosage of Co/C-50 increased from 0.0050 g to 0.0070 g, the  $k_1$  value changed from  $0.537$  min $^{-1}$  to  $0.579$  min $^{-1}$ ; the removal efficiency of BPA was not significantly improved due to the delay of mass transfer and unavailability of active sites in the presence of excessive catalyst.<sup>39</sup> This phenomenon was also shown in the Co/C-50-PDS system (Fig. 5c and d). When the dosage of Co/C-50 was changed to 0.04 g and 0.05 g from 0, the  $k_1$  value increased from  $0.00120$  min $^{-1}$  to  $0.558$  min $^{-1}$  and  $0.594$  min $^{-1}$ , respectively. Hence, the optimal Co/C-50 dosages of 0.0050 and 0.0400 g for PMS and PDS activation were chosen for further experiments.

**3.2.3 Effect of different oxidant concentrations.** Fig. 6 shows the influence of different oxidant concentrations ( $[\text{PS}]_0$ ) on BPA degradation. As shown in Fig. 6a and b, with the addition of 0 to  $0.1$  g L $^{-1}$  of PMS, the degradation efficiency of BPA increased rapidly from 7.15% to 80.82%, with the  $k_1$  value increasing from  $0.00398$  to  $0.169$  min $^{-1}$ ; this indicated that the removal of BPA was contributed by oxidative degradation rather than the adsorption of the catalyst. When  $[\text{PMS}]_0$  was changed

from  $0.1$  g L $^{-1}$  to  $0.20$ ,  $0.25$  and  $0.30$  g L $^{-1}$ , the  $k_1$  value increased by 1.20, 2.18 and 2.54 times compared to that of  $0.1$  g L $^{-1}$  of PMS, respectively. With regard to PDS oxidants, the  $k$  values of BPA increased nearly linearly with the increase of the PDS concentration ( $0.1$ – $1.0$  g L $^{-1}$ ), and then the enhancement of the  $k$  values decreased with further rising of the PDS concentration (Fig. 6c and d). This can be explained by the fact that the excess PDS would react with  $\text{SO}_4^{\cdot-}$  and  $\cdot\text{OH}$  to reduce the utilization efficiency of PDS<sup>40</sup> (eqn (2) and (3)). According to the experimental results, the optimal concentrations of PMS and PDS were  $0.25$  g L $^{-1}$  and  $1.0$  g L $^{-1}$ , respectively.



**3.2.4 Effect of initial pH.** Generally speaking, actual water bodies contain a variety of pH values. Therefore, it was very important to evaluate the catalytic activity of the catalysts in the new degradation system to determine whether the organic pollutants could be degraded effectively at various pH values. Therefore, the removal efficiency of BPA was investigated in the Co/C-50-PS system at different initial pH values ( $\text{pH}_0$ ). When  $\text{pH}_0$  was in the range of 3.0–11.0, BPA could be degraded thoroughly within 30 min (Fig. 7a and b). At higher  $\text{pH}_0$  values, the



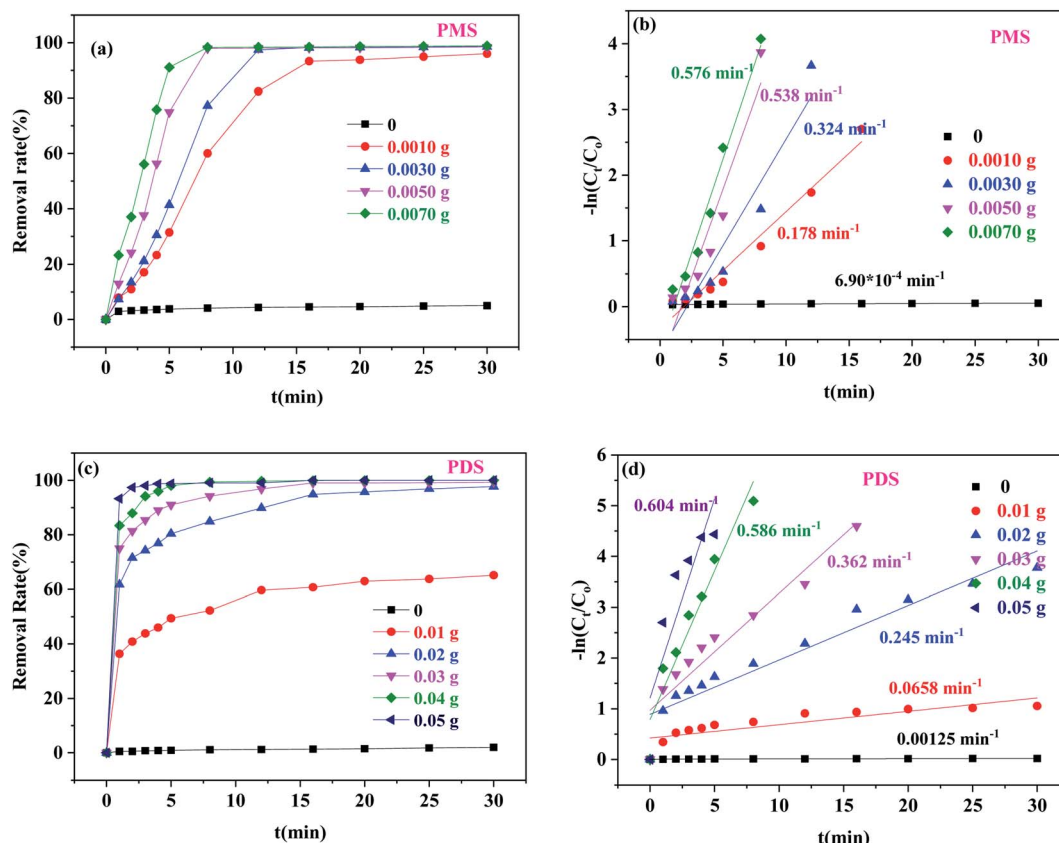
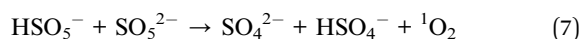
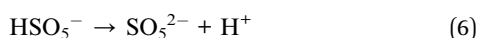
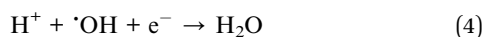
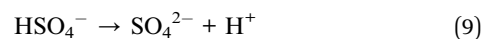
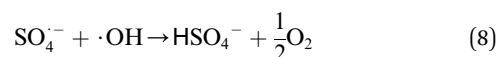


Fig. 5 The effects of Co/C-50 dosage on BPA degradation: removal efficiency of BPA with PMS (a) and PDS (c), and corresponding pseudo-first-order kinetic rate constants (b and d) ([PMS] = 0.25 g L<sup>-1</sup>, [PDS] = 1.0 g L<sup>-1</sup>, [BPA] = 20 mg L<sup>-1</sup>,  $T = 30^\circ\text{C}$ ).

catalytic degradation efficiency of BPA increased significantly. The  $k_1$  value (0.917 min<sup>-1</sup>) of BPA at  $\text{pH}_0 = 11$  was 3.08 times higher than that (0.298 min<sup>-1</sup>) at  $\text{pH}_0 = 3$ . There were five main reasons for this phenomenon: (1) higher leaching of active metal species at lower  $\text{pH}_0$ , reducing the active sites on Co/C-50;<sup>40</sup> (2) the quenching of  $\text{SO}_4^{\cdot-}$  and  $\cdot\text{OH}$  by  $\text{H}^+$  in acidic conditions (eqn (4) and (5));<sup>41</sup> (3) activation of PMS by alkali species;<sup>42</sup> (4) formation of singlet oxygen ( $^1\text{O}_2$ ) due to the decomposition of PMS at higher solution pH (eqn (6) and (7));<sup>43</sup> (5) the increase of the pH value was also conducive to the formation of hydroxyl groups on the surface of the catalyst, which could be used as the active sites for electron transfer, thus improving the performance of the catalyst.<sup>44</sup> Because PDS had the minimum activation energy<sup>45</sup> under neutral conditions, BPA had the highest degradation efficiency at  $\text{pH}_0 = 7$ , and  $k_1$  reached the maximum value of 0.584 min<sup>-1</sup> in the Co/C-50-PDS system (Fig. 7c and d).



After the reaction, the equilibrium pH ( $\text{pH}_e$ ) decreased in varying degrees. In the Co/C-50-PMS system (Fig. 7a), the  $\text{pH}_e$  was 2.53, 2.78, 3.44, 4.97 and 6.39 when  $\text{pH}_0$  was set at 3, 5, 7, 9 and 11, respectively. In the Co/C-50-PDS system (Fig. 7c), the  $\text{pH}_e$  decreased to 2.57, 2.74, 3.68, 4.54 and 7.13, respectively. In addition to releasing protons and forming acidic intermediates during BPA decomposition,<sup>25</sup>  $\text{SO}_4^{\cdot-}$  also reacted with  $\text{H}_2\text{O}$  to form  $\text{H}^+$  (eqn (8) and (9)).<sup>43</sup> Moreover, the PMS itself decomposed to yield  $\text{H}^+$  (eqn (10)).<sup>46</sup>



In general, the Co/C-50-PS system efficiently catalyzed the oxidative removal of BPA under acidic, neutral, and basic conditions, indicating that it has broad application prospects in practical water. The concentration of cobalt ions leached from the reaction solution was determined by ICP-MS. After 30 min reaction in the Co/C-50-PMS system, the concentration of cobalt leaching in the solution was 6.075 mg L<sup>-1</sup>. When the pH value was adjusted to alkaline, almost no cobalt leaching in the solution was observed.





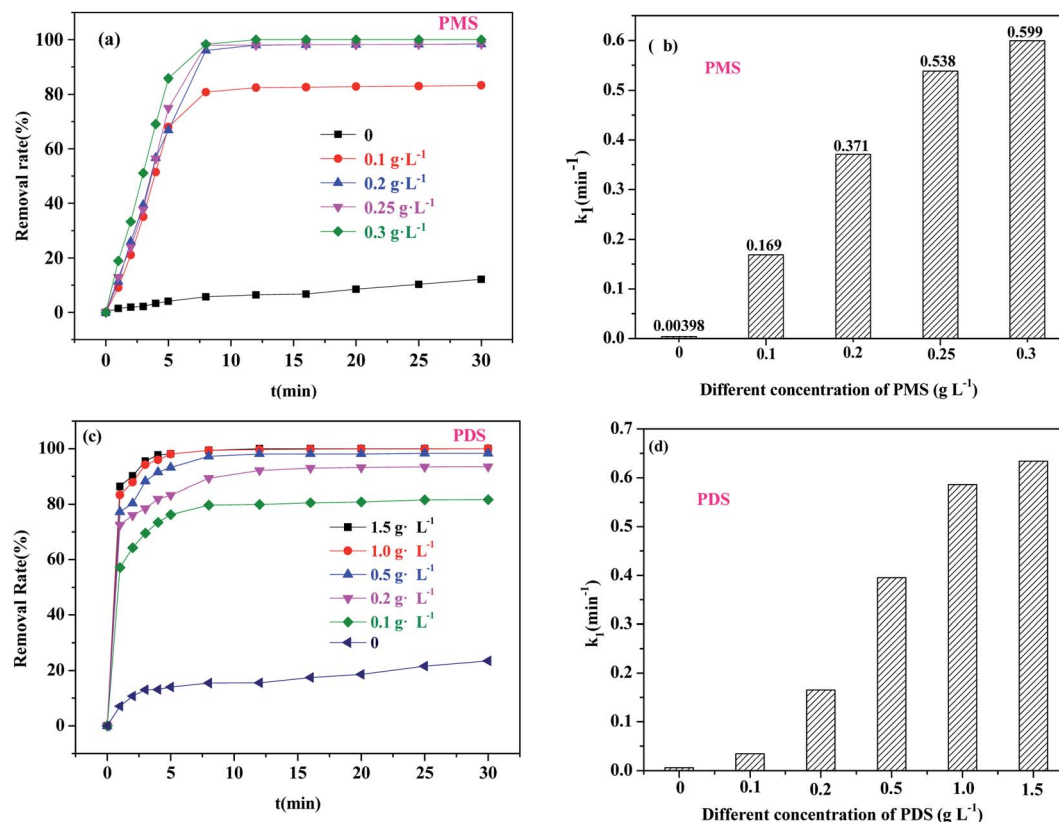


Fig. 6 The effects of PS concentration on BPA degradation: (a and c) BPA degradation as a function of time; (b and d) kinetic constants for BPA degradation (PMS system:  $m_{\text{catalyst}} = 0.0050$  g; PDS system:  $m_{\text{catalyst}} = 0.04$  g, [BPA] =  $20 \text{ mg L}^{-1}$ ,  $T = 30^\circ \text{C}$ ).

The two systems also exhibited high mineralization efficiency (removal of TOC), which was 75% and 90% in Co/C-50-PMS and Co/C-50-PDS, respectively (Text S5 and Fig. S4†). In the Co/C-50-PS system, hydroquinone and benzoquinone should be the major intermediates of BPA.<sup>47–49</sup> The ring of benzoquinone could be further cleaved in the presence of  $\text{SO}_4^{\cdot-}$  and  $\cdot\text{OH}$  radicals to form some small molecular organic acids, such as fumaric acid, malonic acid, and formic acid, which should be responsible for the residual TOC.

**3.2.5 Effects of reaction temperature and reusability of the Co/C-50 catalyst.** The degradation of BPA was fast and efficient under the temperatures of  $15^\circ \text{C}$ ,  $30^\circ \text{C}$  and  $45^\circ \text{C}$ , and the fitting reaction activation energies ( $E_a$ ) were small, which was conducive to trigger the reaction under mild conditions (Text S6 and Fig. S5†). The removal efficiency of BPA remained above 90% after five cycles, exhibiting good reusability of the Co/C-50 catalyst (Text S7 and Fig. S6†).

**3.2.6 Effects of the actual water matrix and different target pollutants.** Despite the matrix interference, the Co/C-50-PS system exhibited good efficiency for BPA degradation in different actual water samples (Text S8 and Fig. S7†). The results of the Co/C-50-PS system for removal of different pollutants are shown in Text S9 and Fig. S8†.

**3.2.7 Free radical quenching experiment and ESR analysis.** Previous studies suggested that  $\text{SO}_4^{\cdot-}$  and  $\cdot\text{OH}$  are the main active substances for the activation of PS by metal-based

catalysts.<sup>50</sup> Consequently, the contribution of free radicals to BPA removal was studied by the free radical quenching method. Methanol (MeOH), as an alcohol containing  $\alpha\text{-H}$ , has a similar reaction efficiency to  $\cdot\text{OH}$  and  $\text{SO}_4^{\cdot-}$  (eqn (11) and (12)),<sup>51</sup> and the reaction efficiency of *tert*-butyl alcohol (TBA) without  $\alpha\text{-H}$  with  $\cdot\text{OH}$  is 3 orders higher than that of  $\text{SO}_4^{\cdot-}$  (eqn (13) and (14)).<sup>52</sup> Therefore, MeOH was used to quench  $\cdot\text{OH}$  and  $\text{SO}_4^{\cdot-}$ , TBA was used to quench  $\cdot\text{OH}$  and  $\text{Na}_2\text{S}_2\text{O}_3$  was used to quench surface free radicals.

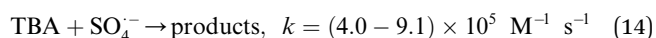
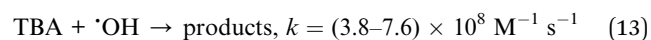
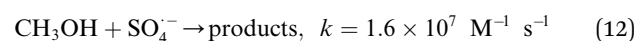
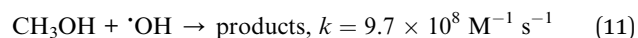


Fig. 8 shows the degradation efficiency of BPA in pure water, MeOH-aqueous solution, TBA-aqueous solution, and  $\text{Na}_2\text{S}_2\text{O}_3$ -aqueous solution. In the Co/C-50-PMS system (Fig. 8a), the removal efficiencies of BPA in pure water, MeOH-aqueous solution, TBA-aqueous solution, and  $\text{Na}_2\text{S}_2\text{O}_3$ -aqueous solution were 100%, 27.84%, 68.09%, and 10.14%, and the  $k_1$  values were 0.522, 0.00893, 0.0388, and 0.00225 min<sup>-1</sup>, respectively. Compared with TBA, BPA had a lower degradation efficiency and  $k_1$  value with MeOH addition, which indicated that  $\text{SO}_4^{\cdot-}$



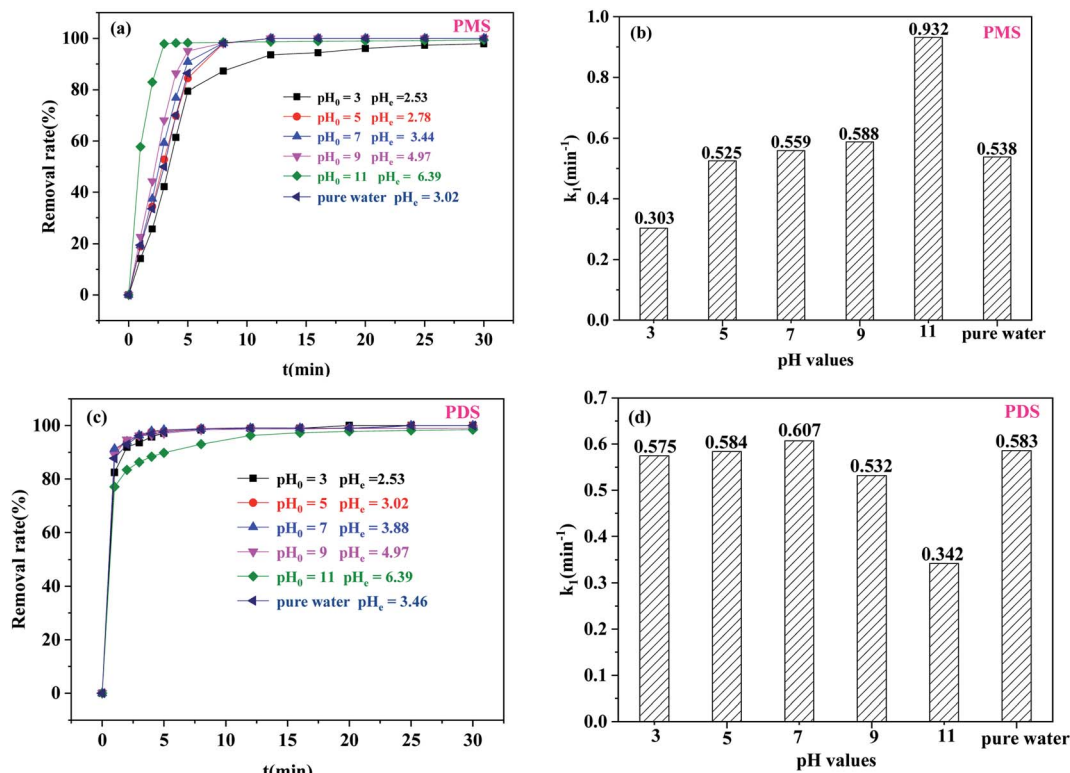


Fig. 7 The effect of solution pH: (a and b) PMS system ( $m_{\text{catalyst}} = 0.0050$  g,  $[\text{PMS}] = 0.25$  g L<sup>-1</sup>); (c and d) PDS system ( $m_{\text{catalyst}} = 0.04$  g,  $[\text{PDS}] = 1.0$  g L<sup>-1</sup>) ([BPA] = 20 mg L<sup>-1</sup>,  $T = 30$  °C).

was the primary active radical. In the Co/C-50-PDS system (Fig. 8b), the removal efficiencies of BPA in pure water, MeOH-aqueous solution, TBA-aqueous solution, and Na<sub>2</sub>S<sub>2</sub>O<sub>3</sub>-aqueous solution were 100%, 100%, 78.97% and 25.78%, respectively, and the corresponding  $k_1$  values were 0.586 min<sup>-1</sup>, 0.313 min<sup>-1</sup>, 0.0684 min<sup>-1</sup> and 0.00917 min<sup>-1</sup>, respectively. Different from the PMS system, BPA had a lower removal efficiency and  $k_1$  value with TBA addition; this indicated that  $\cdot\text{OH}$  was the dominant radical for BPA degradation, while  $\cdot\text{OH}$  was produced by the reaction of  $\text{SO}_4^{\cdot-}$  with  $\text{H}_2\text{O}/\text{OH}^-$ .<sup>53</sup>

In addition, BPA had the lowest removal efficiency in Co/C-50-PS-Na<sub>2</sub>S<sub>2</sub>O<sub>3</sub>, indicating that surface free radicals played a key role in the degradation process.<sup>50</sup>

Electron spin resonance (ESR, A300 microx, Bruker, Germany) was used to detect free radicals in the Co/C-50-PS system. DMPO is a spin trapping agent for  $\text{SO}_4^{\cdot-}$  and  $\cdot\text{OH}$ , and TEMP is a spin trapping agent for  $^1\text{O}_2$ . No free radical signal was detected when only DMPO was added to the solution containing PS, and DMPO- $\cdot\text{OH}$  and DMPO- $\text{SO}_4^{\cdot-}$  signal peaks appeared after the Co/C-50 catalyst was added for a period of time (Fig. 9a and b).<sup>54</sup>

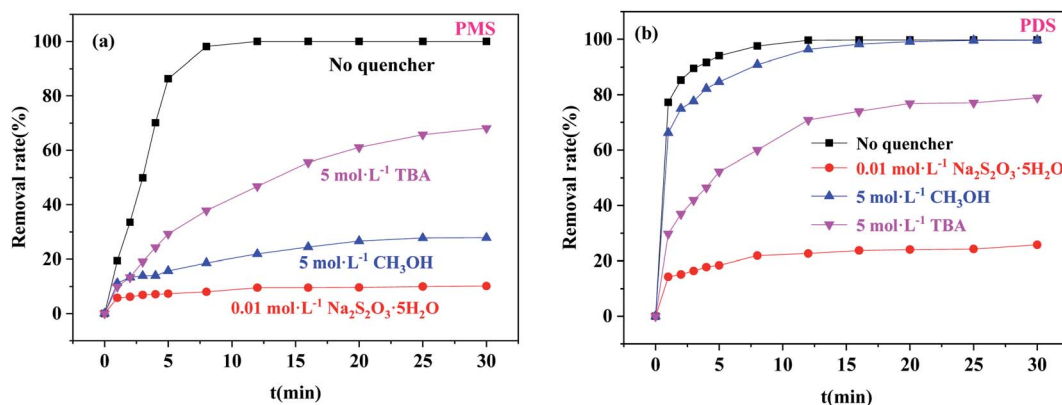


Fig. 8 Free radical annihilation experiment: (a) PMS system ( $m_{\text{catalyst}} = 0.0050$  g,  $[\text{PMS}] = 0.25$  g L<sup>-1</sup>); (b) PDS system ( $m_{\text{catalyst}} = 0.04$  g,  $[\text{PDS}] = 1.0$  g L<sup>-1</sup>) ([BPA] = 20 mg L<sup>-1</sup>,  $T = 30$  °C).



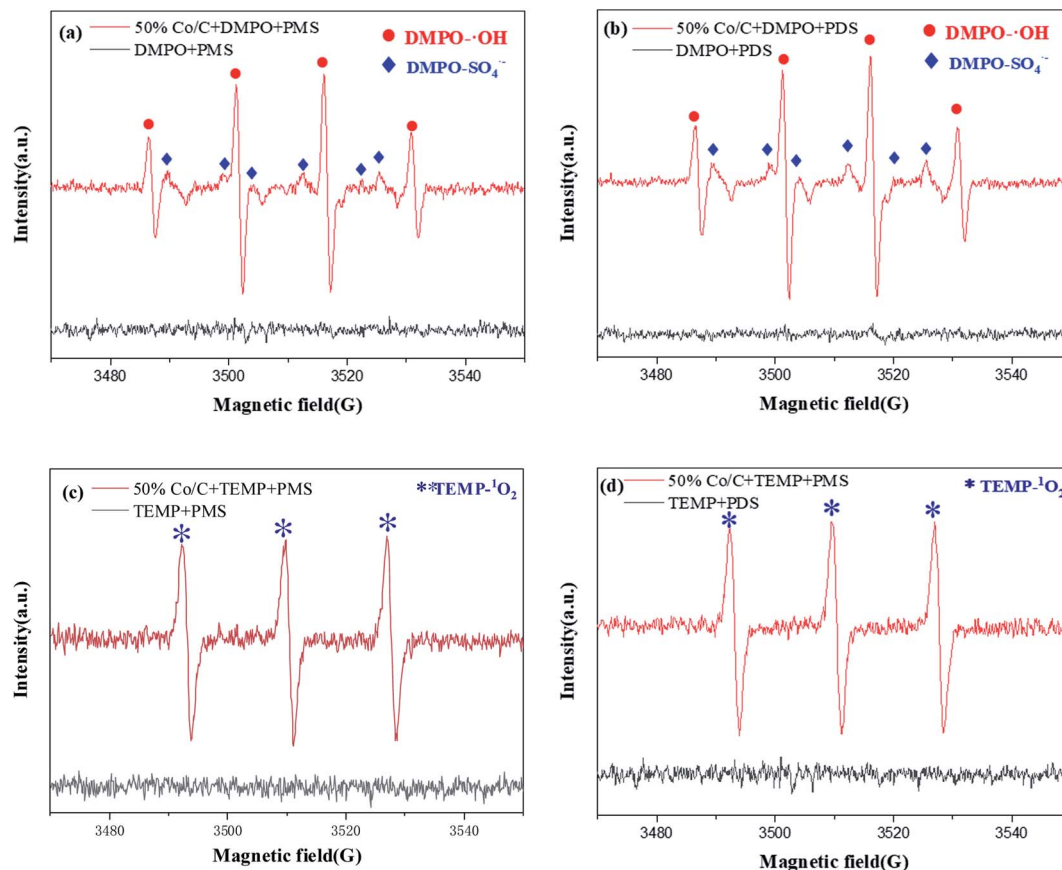


Fig. 9 ESR spectra of PMS and PDS activation by Co/C-50. (a) DMPO- $\cdot\text{OH}$  and DMPO- $\text{SO}_4^{\cdot-}$  (PMS); (b) DMPO- $\cdot\text{OH}$  and  $\text{SO}_4^{\cdot-}$  (PDS); (c) TEMP- $^1\text{O}_2$  (PMS); (d) TEMP- $^1\text{O}_2$  (PDS) spin adducts (PMS system:  $m_{\text{catalyst}} = 0.0050$  g,  $[\text{PMS}] = 0.25$  g  $\text{L}^{-1}$ ; PDS system:  $m_{\text{catalyst}} = 0.04$  g,  $[\text{PDS}] = 1.0$  g  $\text{L}^{-1}$ ).

Similarly, only TEMP was added to the solution containing PS, and no free radical signal was detected. After adding the Co/C-50 catalyst, the signal peak of TEMP- $^1\text{O}_2$  appeared (Fig. 9c and d).<sup>55</sup> This indicated that Co/C-50 can indeed activate PS to produce  $\text{SO}_4^{\cdot-}$ ,  $\cdot\text{OH}$  and  $^1\text{O}_2$ .

## 4. Conclusion

In this study, a Co/C composite was successfully established by one-step activation pyrolysis, and the material exhibited great performance for the degradation and mineralization of BPA by activating PMS and PDS. The reactive oxygen species (ROS) involved in BPA degradation comprised  $\text{SO}_4^{\cdot-}$ ,  $\cdot\text{OH}$  and  $^1\text{O}_2$ . This new type of cobalt-based heterogeneous catalyst possessed excellent pH adaptability, practical application performance, and reusability for removal of organic pollutants.

## Conflicts of interest

There are no conflicts to declare.

## Acknowledgements

This work was jointly supported by the Science and Technology Innovation Development Program of Yantai (2022YT06000734),

the National Natural Science Foundation of China (21207059) and the Natural Science Foundation of Shandong Province (ZR2011BQ012).

## References

- 1 X. Guo, Y. Huang, W. Yu, X. Yu, X. Han and H. Zhai, Multi-walled carbon nanotubes modified with iron oxide and manganese dioxide (MWCNTs- $\text{Fe}_3\text{O}_4$ - $\text{MnO}_2$ ) as a novel adsorbent for the determination of BPA, *Microchem. J.*, 2020, **157**, 104867.
- 2 L. Wang, J. Yun, H. Zhang, J. Si, X. Fang and L. Shao, Degradation of Bisphenol A by ozonation in rotating packed bed: Effects of operational parameters and co-existing chemicals, *Chemosphere*, 2021, **274**, 129769.
- 3 G. Ji, J. Gu, M. Guo, L. Zhou, Z. Wang, L. Shi and A. Gu, A systematic comparison of the developmental vascular toxicity of bisphenol A and its alternatives *in vivo* and *in vitro*, *Chemosphere*, 2021, 132936.
- 4 S. Wang, S. Chen, Y. Wang, A. Low, Q. Lu and R. Qiu, Integration of organohalide-respiring bacteria and nanoscale zero-valent iron (Bio-nZVI-RD): A perfect marriage for the remediation of organohalide pollutants?, *Biotechnol. Adv.*, 2016, **34**(8), 1384–1395.



- 5 S. I. Kaya, A. Cetinkaya and S. A. Ozkan, Latest advances on the nanomaterials-based electrochemical analysis of azo toxic dyes Sunset Yellow and Tartrazine in food samples, *Food Chem. Toxicol.*, 2021, **156**, 112524.
- 6 I. Michael, A. Achilleos, D. Lambropoulou, V. O. Torrens, S. Pérez, M. Petrović, D. Barceló and D. Fatta-Kassinos, Proposed transformation pathway and evolution profile of diclofenac and ibuprofen transformation products during (sono)photocatalysis, *Appl. Catal., B*, 2014, **147**, 1015–1027.
- 7 E. Li, D. G. Bolser, K. J. Kroll, E. K. Brockmeier, F. Falciani and N. D. Denslow, Comparative toxicity of three phenolic compounds on the embryo of fathead minnow, *Pimephales promelas*, *Aquat. Toxicol.*, 2018, **201**, 66–72.
- 8 X. Xu, Y. Feng, Z. Chen, S. Wang, G. Wu, T. Huang, J. Ma and G. Wen, Activation of peroxymonosulfate by  $\text{CuCo}_2\text{O}_4$ -GO for efficient degradation of bisphenol A from aqueous environment, *Sep. Purif. Technol.*, 2020, **251**, 117351.
- 9 X. L. Chen, F. Li, M. Zhang, B. Liu, H. Chen and H. Wang, Highly dispersed and stabilized  $\text{Co}_3\text{O}_4/\text{C}$  anchored on porous biochar for bisphenol A degradation by sulfate radical advanced oxidation process, *Sci. Total Environ.*, 2021, 777, 145794.
- 10 X. Li, S. Zhang, M. Yu, H. Xu, J. Lv, S. Yang, X. Zhu and L. Li, One-pot pyrolysis method for synthesis of Fe/N co-doped biochar as an effective peroxymonosulfate activator for RhB degradation, *J. Taiwan Inst. Chem. Eng.*, 2021, **128**, 209–219.
- 11 X. Lou, L. Wu, Y. Guo, C. Chen, Z. Wang, D. Xiao, C. Fang, J. Liu, J. Zhao and S. Lu, Peroxymonosulfate activation by phosphate anion for organics degradation in water, *Chemosphere*, 2014, **117**, 582–585.
- 12 V. T. Nguyen, T. B. Nguyen, C. W. Chen, C. M. Hung, C. P. Huang and C. D. Dong, Cobalt-impregnated biochar (Co-SCG) for heterogeneous activation of peroxymonosulfate for removal of tetracycline in water, *Bioresour. Technol.*, 2019, **292**, 121954.
- 13 G. D. Fang, D. D. Dionysiou, Y. Wang, S. R. Al-Abed and D. M. Zhou, Sulfate radical-based degradation of polychlorinated biphenyls: effects of chloride ion and reaction kinetics, *J. Hazard. Mater.*, 2012, **227–228**, 394–401.
- 14 S. Wacławek, H. V. Lutze, K. Gröbel, V. V. T. Padil, M. Černík and D. D. Dionysiou, Chemistry of persulfates in water and wastewater treatment: A review, *Chem. Eng. J.*, 2017, **330**, 44–62.
- 15 T. Olmez-Hanci, I. Arslan-Alaton and B. Genc, Bisphenol A treatment by the hot persulfate process: oxidation products and acute toxicity, *J. Hazard. Mater.*, 2013, **263**, 283–290.
- 16 C. Qi, X. Liu, C. Lin, X. Zhang, J. Ma, H. Tan and W. Ye, Degradation of sulfamethoxazole by microwave-activated persulfate: Kinetics, mechanism and acute toxicity, *Chem. Eng. J.*, 2014, **249**, 6–14.
- 17 Y. Wang, Z. Gu, S. Yang and A. Zhang, Activation of persulfate by microwave radiation combined with FeS for treatment of wastewater from explosives production, *Environ. Sci.: Water Res. Technol.*, 2020, **6**(3), 581–592.
- 18 Z. Wei, F. A. Villamena and L. K. Weavers, Kinetics and Mechanism of Ultrasonic Activation of Persulfate: An *in Situ* EPR Spin Trapping Study, *Environ. Sci. Technol.*, 2017, **51**(6), 3410–3417.
- 19 J. Sharma, I. M. Mishra, D. D. Dionysiou and V. Kumar, Oxidative removal of Bisphenol A by UV-C/peroxymonosulfate (PMS): Kinetics, influence of co-existing chemicals and degradation pathway, *Chem. Eng. J.*, 2015, **276**, 193–204.
- 20 J. Molnar Jazić, T. Đurkić, B. Bašić, M. Watson, T. Apostolović, A. Tubić and J. Agbaba, Degradation of a chloroacetanilide herbicide in natural waters using UV activated hydrogen peroxide, persulfate and peroxymonosulfate processes, *Environ. Sci.: Water Res. Technol.*, 2020, **6**(10), 2800–2815.
- 21 C. S. Liu, K. Shih, C. X. Sun and F. Wang, Oxidative degradation of propachlor by ferrous and copper ion activated persulfate, *Sci. Total Environ.*, 2012, **416**, 507–512.
- 22 Y. Wan, J. Ye, L. Wang and J. Dai, Interfacial engineering for ultrafine  $\text{Co}_3\text{O}_4$  confined in graphene macroscopic microspheres with boosting peroxymonosulfate activation, *J. Taiwan Inst. Chem. Eng.*, 2021, **127**, 248–258.
- 23 X. Duan, H. Sun, J. Kang, Y. Wang, S. Indrawirawan and S. Wang, Insights into Heterogeneous Catalysis of Persulfate Activation on Dimensional-Structured Nanocarbons, *ACS Catal.*, 2015, **5**(8), 4629–4636.
- 24 X.-Y. Pei, H.-Y. Ren, D.-F. Xing, G.-J. Xie, G.-L. Cao, J. Meng, N.-Q. Ren and B.-F. Liu, Electron transfer mechanism of peroxydisulfate activation by sewage sludge-derived biochar for enhanced degradation of sulfamethoxazole, *Environ. Sci.: Water Res. Technol.*, 2021, **7**(9), 1563–1575.
- 25 C. Qi, X. Liu, J. Ma, C. Lin, X. Li and H. Zhang, Activation of peroxymonosulfate by base: Implications for the degradation of organic pollutants, *Chemosphere*, 2016, **151**, 280–288.
- 26 K. A. Lin and B. J. Chen, Prussian blue analogue derived magnetic carbon/cobalt/iron nanocomposite as an efficient and recyclable catalyst for activation of peroxymonosulfate, *Chemosphere*, 2017, **166**, 146–156.
- 27 Q. Gao, G. Wang, Y. Chen, B. Han, K. Xia and C. Zhou, Utilizing cobalt-doped materials as heterogeneous catalysts to activate peroxymonosulfate for organic pollutant degradation: a critical review, *Environ. Sci.: Water Res. Technol.*, 2021, **7**(7), 1197–1211.
- 28 K. Liu, M. Li, Z. Zhu, B. Gao, H. Zeng, Y. Ma and L. Fang, Emerging investigator series: 3D graphene anchored zerovalent Fe/Cu aerogel activating persulfate for efficiently 2,4 dichlorophenol degradation over a broad pH range, *Environ. Sci.: Water Res. Technol.*, 2021, **7**(4), 714–725.
- 29 P. Hu and M. Long, Cobalt-catalyzed sulfate radical-based advanced oxidation: A review on heterogeneous catalysts and applications, *Appl. Catal., B*, 2016, **181**, 103–117.
- 30 D. Ding, S. Yang, X. Qian, L. Chen and T. Cai, Nitrogen-doping positively whilst sulfur-doping negatively affect the catalytic activity of biochar for the degradation of organic contaminant, *Appl. Catal., B*, 2020, **263**, 118348.
- 31 D. Yu, L. Zhou, J. Hu, C. Peng and H. Liu, Facile synthesis of nitrogen, sulfur dual-doped porous carbon *via* carbonization



- of coal tar pitch and  $\text{MgCl}_2 \cdot 6\text{H}_2\text{O}$  for oxygen reduction reaction, *J. Solid State Electrochem.*, 2019, **23**(8), 2455–2464.
- 32 M. Wang, Y. Cui, H. Cao, P. Wei, C. Chen, X. Li, J. Xu and G. Sheng, Activating peroxydisulfate with  $\text{Co}_3\text{O}_4/\text{NiCo}_2\text{O}_4$  double-shelled nanocages to selectively degrade bisphenol A – A nonradical oxidation process, *Appl. Catal., B*, 2021, **282**, 119585.
  - 33 G. Wei, X. Liang, Z. He, Y. Liao, Z. Xie, P. Liu, S. Ji, H. He, D. Li and J. Zhang, Heterogeneous activation of Oxone by substituted magnetites  $\text{Fe}_{3-x}\text{M}_x\text{O}_4$  (Cr, Mn, Co, Ni) for degradation of Acid Orange II at neutral pH, *J. Mol. Catal. A: Chem.*, 2015, **398**, 86–94.
  - 34 T. Zhan, Y. Zhang, X. Liu, S. Lu and W. Hou, NiFe layered double hydroxide/reduced graphene oxide nanohybrid as an efficient bifunctional electrocatalyst for oxygen evolution and reduction reactions, *J. Power Sources*, 2016, **333**, 53–60.
  - 35 S. Li, Z. Jiang, X. Xiao, W. Chen, X. Tian, X. Hao and Z.-J. Jiang, MOF-derived Co nanoparticles embedded in N,S-codoped carbon layer/MWCNTs for efficient oxygen reduction in alkaline media, *Ionics*, 2018, **25**(2), 785–796.
  - 36 Z. Zhen, Z. Jiang, X. Tian, L. Zhou, B. Deng, B. Chen and Z.-J. Jiang, Core@shell structured Co–CoO@NC nanoparticles supported on nitrogen doped carbon with high catalytic activity for oxygen reduction reaction, *RSC Adv.*, 2018, **8**(26), 14462–14472.
  - 37 M. Xie, J. Tang, L. Kong, W. Lu, V. Natarajan, F. Zhu and J. Zhan, Cobalt doped g- $\text{C}_3\text{N}_4$  activation of peroxymonosulfate for monochlorophenols degradation, *Chem. Eng. J.*, 2019, **360**, 1213–1222.
  - 38 M. Pu, Y. Ma, J. Wan, Y. Wang, M. Huang and Y. Chen, Fe/S doped granular activated carbon as a highly active heterogeneous persulfate catalyst toward the degradation of Orange G and diethyl phthalate, *J. Colloid Interface Sci.*, 2014, **418**, 330–337.
  - 39 N. Zhou, J. Zu, L. Yang, X. Shu, J. Guan, Y. Deng, D. Gong, C. Ding and M. E. Zhong, Cobalt (0/II) incorporated N-doped porous carbon as effective heterogeneous peroxymonosulfate catalyst for quinclorac degradation, *J. Colloid Interface Sci.*, 2020, **563**, 197–206.
  - 40 J. Du, J. Bao, Y. Liu, S. H. Kim and D. D. Dionysiou, Facile preparation of porous  $\text{Mn}/\text{Fe}_3\text{O}_4$  cubes as peroxymonosulfate activating catalyst for effective bisphenol A degradation, *Chem. Eng. J.*, 2019, **376**, 119193.
  - 41 Y. H. Huang, Y. F. Huang, C. I. Huang and C. Y. Chen, Efficient decolorization of azo dye Reactive Black B involving aromatic fragment degradation in buffered  $\text{Co}^{2+}$ /PMS oxidative processes with a ppb level dosage of  $\text{Co}^{2+}$ -catalyst, *J. Hazard. Mater.*, 2009, **170**(2–3), 1110–1118.
  - 42 O. S. T. a L. Furman and R. J. Watts, Mechanism of Base Activation of Persulfate, *Environ. Sci. Technol.*, 2010, **44**, 6423–6428.
  - 43 S. Su, W. Guo, Y. Leng, C. Yi and Z. Ma, Heterogeneous activation of Oxone by  $\text{Co}_x\text{Fe}_{3-x}\text{O}_4$  nanocatalysts for degradation of rhodamine B, *J. Hazard. Mater.*, 2013, **244–245**, 736–742.
  - 44 Y. Lei, C. S. Chen, Y. J. Tu, Y. H. Huang and H. Zhang, Heterogeneous Degradation of Organic Pollutants by Persulfate Activated by  $\text{CuO}-\text{Fe}_3\text{O}_4$ : Mechanism, Stability, and Effects of pH and Bicarbonate Ions, *Environ. Sci. Technol.*, 2015, **49**(11), 6838–6845.
  - 45 H. Yin, F. Yao, Z. Pi, Y. Zhong, L. He, K. Hou, J. Fu, S. Chen, Z. Tao, D. Wang, X. Li and Q. Yang, Efficient degradation of bisphenol A via peroxydisulfate activation using *in situ* N-doped carbon nanoparticles: Structure-function relationship and reaction mechanism, *J. Colloid Interface Sci.*, 2021, **586**, 551–562.
  - 46 C. Cai, H. Zhang, X. Zhong and L. Hou, Ultrasound enhanced heterogeneous activation of peroxymonosulfate by a bimetallic Fe-Co/SBA-15 catalyst for the degradation of Orange II in water, *J. Hazard. Mater.*, 2015, **283**, 70–79.
  - 47 I. Hussain, Y. Zhang and S. Huang, Degradation of aniline with zero-valent iron as an activator of persulfate in aqueous solution, *RSC Adv.*, 2014, **4**(7), 3502–3511.
  - 48 X. Li, S. Zhang, M. Zhang, M. Yu, H. Chen, H. Yang and Q. Xu, One-step synthesis of mixed valence FeOX nanoparticles supported on biomass activated carbon for degradation of bisphenol A by activating peroxydisulfate, *J. Hazard. Mater.*, 2021, **409**, 124990.
  - 49 D. Chen, K. Kannan, H. Tan, Z. Zheng, Y. L. Feng, Y. Wu and M. Widelka, Bisphenol Analogues Other Than BPA: Environmental Occurrence, Human Exposure, and Toxicity-A Review, *Environ. Sci. Technol.*, 2016, **50**(11), 5438–5453.
  - 50 T. Zeng, S. Li, J. Hua, Z. He, X. Zhang, H. Feng and S. Song, Synergistically enhancing Fenton-like degradation of organics by *in situ* transformation from  $\text{Fe}_3\text{O}_4$  microspheres to mesoporous Fe, N-dual doped carbon, *Sci. Total Environ.*, 2018, **645**, 550–559.
  - 51 F. Gong, L. Wang, D. Li, F. Zhou, Y. Yao, W. Lu, S. Huang and W. Chen, An effective heterogeneous iron-based catalyst to activate peroxymonosulfate for organic contaminants removal, *Chem. Eng. J.*, 2015, **267**, 102–110.
  - 52 Y. Qian, G. Xue, J. Chen, J. Luo, X. Zhou, P. Gao and Q. Wang, Oxidation of cefalexin by thermally activated persulfate: Kinetics, products, and antibacterial activity change, *J. Hazard. Mater.*, 2018, **354**, 153–160.
  - 53 Y. Zhou, X. Wang, C. Zhu, D. D. Dionysiou, G. Zhao, G. Fang and D. Zhou, New insight into the mechanism of peroxymonosulfate activation by sulfur-containing minerals: Role of sulfur conversion in sulfate radical generation, *Water Res.*, 2018, **142**, 208–216.
  - 54 B. Jiang, X. Wang, Y. Liu, Z. Wang, J. Zheng and M. Wu, The roles of polycarboxylates in Cr(VI)/sulfite reaction system: Involvement of reactive oxygen species and intramolecular electron transfer, *J. Hazard. Mater.*, 2016, **304**, 457–466.
  - 55 R. Yuan, M. Jiang, S. Gao, Z. Wang, H. Wang, G. Boczkaj, Z. Liu, J. Ma and Z. Li, 3D mesoporous  $\alpha\text{-Co}(\text{OH})_2$  nanosheets electrodeposited on nickel foam: A new generation of macroscopic cobalt-based hybrid for peroxymonosulfate activation, *Chem. Eng. J.*, 2020, **380**, 122447.

